Disorder-induced spin excitation continuum and spin-glass ground state in the inverse spinel $CuGa_2O_4$

Zhentao Huang,[1,*] Zhijun Xu,[2,*] Shuaiwei Li,[3] Qingchen Duan,[4] Junbo Liao,[1] Song Bao,[1] Yanyan Shangguan,[1] Bo Zhang,[1] Hao Xu,[1] Shufan Cheng,[1] Zihang Song,[1] Shuai Dong,[1] Maofeng Wu,[1] M. B. Stone,[5] Yiming Qiu,[2] Ruidan Zhong,[4] Guangyong Xu,[2] Zhen Ma,[1,3,†] G. D. Gu,[6,‡] J. M. Tranquada,[6,§] and Jinsheng Wen[1,7,‖]

[1]*National Laboratory of Solid State Microstructures and Department of Physics, Nanjing University, Nanjing 210093, China*

[2]*NIST Center for Neutron Research, National Institute of Standards and Technology, Gaithersburg, Maryland 20899, USA*

[3]*Hubei Key Laboratory of Photoelectric Materials and Devices, School of Materials Science and Engineering, Hubei Normal University, Huangshi 435002, China*

[4]*Tsung-Dao Lee Institute & School of Physics and Astronomy, Shanghai Jiao Tong University, Shanghai 200240, China*

[5]*Neutron Scattering Division, Oak Ridge National Laboratory, Oak Ridge, Tennessee 37831, USA*

[6]*Condensed Matter Physics and Materials Science Division, Brookhaven National Laboratory, Upton, New York 11973-5000, USA*

[7]*Collaborative Innovation Center of Advanced Microstructures and Jiangsu Physical Science Research Center, Nanjing University, Nanjing 210093, China*

(Received 7 April 2025; revised 11 June 2025; accepted 24 June 2025; published 10 July 2025)

Spinel-structured compounds serve as prototypical examples of highly frustrated systems and are promising candidates for realizing the long-sought quantum spin liquid (QSL) state. However, structural disorder is inevitable in many real QSL candidates and its impact remains a topic of intense debate. In this work, we conduct comprehensive investigations on $CuGa_2O_4$, a spinel compound with significant structural disorder, focusing on its thermodynamic properties and spectroscopic behaviors. No long-range magnetic order is observed down to ~80 mK, as evidenced by magnetic susceptibility, specific-heat, and elastic neutron scattering measurements. More intriguingly, inelastic neutron scattering experiments reveal a broad gapless continuum of magnetic excitations around the Brillouin zone boundary, resembling the magnetic excitation spectra expected for a QSL. Nevertheless, a spin-freezing transition at $T_f \approx 0.88$ K is identified from the cusp in the dc susceptibility curves, where a bifurcation between zero-field-cooling and field-cooling curves occurs. Furthermore, ac susceptibility measurements show a peak close to T_f at low frequency, which shifts to higher temperature with increasing frequency. These results show that $CuGa_2O_4$ has a spin-glass ground state, consistent with the establishment of short-range order inferred from the specific-heat measurements. Collectively, these results illustrate the crucial role of disorder in defining the excitation spectrum out of the disordered ground state. Our findings shed light onto the broader class of AB_2O_4 spinels and advance our understanding of the spin dynamics in magnetically disordered systems.

DOI: 10.1103/1xtf-wg3q

I. INTRODUCTION

Frustrated systems represent a fascinating frontier in condensed matter physics, where competing interactions give rise to quantum fluctuations, resulting in rich emergent phenomena [1–3]. Of particular interest are quantum spin liquids (QSLs), in which strong quantum fluctuations prevent the establishment of conventional long-range magnetic order, but can also give rise to fractionalized quasiparticle excitations such as spinons [3–8]. Frustration typically arises from geometrical constraints, as in triangular or kagome lattices [9,10], or from competing exchange interactions, as in the honeycomb lattice [11–13]. Within the landscape of frustrated systems, the compounds with a AB_2X_4 (A = transition metal, B = Al, Ga, Sc; X = O, S) spinel structure stand out as prototypical examples due to their inherent geometrical and magnetic structures [14–18]. These materials have attracted significant attention for their potential to host novel quantum states [16,19–21].

The AB_2X_4 family of compounds crystallizes in the cubic spinel structure (space group $Fd\bar{3}m$), where A-site cations occupy tetrahedral coordination sites, while B-site cations reside at the octahedral coordination sites. If the magnetic ions are located at the A sites, such compounds are termed A-site magnetic spinels. Here, the magnetic ions at the A sites form a diamondlike magnetic lattice, resulting in various exotic phenomena depending on the ratio of the next-nearest-neighbor interaction (J_2) to the nearest-neighbor interaction (J_1) [16]. This has been the subject of extensive investigations in recent years [17,18,20,22–24]. A notable example is the spiral spin liquid state observed in the highly frustrated

*These authors contributed equally to this work.
†Contact author: zma@hbnu.edu.cn
‡Contact author: ggu@bnl.gov
§Contact author: jtran@bnl.gov
‖Contact author: jwen@nju.edu.cn

 ©2025 American Physical Society

compound $MnSc_2S_4$ with $|J_2/J_1| = 0.85$ (Refs. [16,25]). $CuAl_2O_4$ has also attracted a lot of attention with A sites nominally occupied by Cu^{2+} with spin-1/2 [26,27]. With Cu^{2+} in a tetrahedrally coordinated site, the single $3d$ hole should be shared among the threefold degenerate t_{2g} orbitals. Taking spin-orbital coupling into account, it might be possible to realize a spin-orbital-liquid ground state [26]. Unfortunately, a study with resonant inelastic x-ray spectroscopy found evidence that the A site has a Jahn-Teller distortion, inconsistent with spin-orbital coupling, and that Cu is also present at the octahedral B site [28].

Most investigations on the spinel compounds have focused on the normal A-site magnetic spinels [16–18,20,22–27], while those with inverse spinel structure have received relatively little attention. In reality, site mixing is a common phenomenon in spinel structures, where a fraction of A- and B-site cations interchange positions. This can introduce a high degree of antisite disorder and, in the extreme case, can lead to the formation of an inverse spinel structure, where all the original A-site magnetic ions sit on the B sites [29]. The extent of this antisite disorder can be quantified by the inversion parameter δ, which is expressed as $(A_{1-\delta}B_{\delta})[B_{2-\delta}A_{\delta}]X_4$ [14,20,26]. Here, parentheses denote the tetrahedral coordination site, while brackets indicate the octahedral coordination site. The closer the inversion parameter δ is to 0.5, the stronger is the degree of antisite disorder. Note that in the case of $CuAl_2O_4$, experiments indicate that $\delta \approx 0.3$ (Refs. [28,30,31]). It is noteworthy that such antisite disorder is typically regarded as an obstacle to the formation of QSLs [6,8], while others suggest that disorder can, in some cases, play a crucial role in stabilizing the QSL phase [18,32,33].

In this work, we study $CuGa_2O_4$, an inverse spinel compound in which a significant fraction of Cu^{2+} ions occupy octahedral B sites rather than tetrahedral A sites. The site disorder has been considered to play a crucial role in determining the physical properties [34,35]. To elucidate the underlying physics and clarify the impact of disorder in the magnetic ground state, we perform neutron scattering experiments, complemented by magnetization and specific-heat measurements. Our results show that there is no long-range magnetic order down to ∼80 mK, but there is a broad gapless continuum of spin excitations as expected for a QSL [9,36–38]. However, both dc and ac susceptibility measurements reveal a spin-freezing transition at low temperatures, with $T_f \approx 0.88$ K determined from the dc susceptibility and a frequency-dependent peak in the real part of the ac susceptibility. This freezing temperature is close to the broad hump around 1 K observed in the specific heat, suggesting the development of short-range magnetic correlations near T_f. These results evidence that $CuGa_2O_4$ is a spin glass where disorder plays a crucial role.

II. EXPERIMENTAL DETAILS

Crystals of $CuGa_2O_4$ were grown by the floating-zone method. To prepare the feed rod, powders of high-purity Ga_2O_3 (99.99%) and CuO (99.99%) were mixed in the ratio of 1.085:1 (where the excess Ga allows for evaporation during the single-crystal growth process), ground, and calcined for 48 h at 1150 °C. The reground powders were placed in a rubber tube and hydrostatically pressed under 6000 kg/cm^2. The pressed rods, with 8 mm diameter, were sintered for 72 h at 1350 °C for use as feed rods. The single-crystal rod was grown at a velocity of 0.4 mm/h in 1 bar oxygen flow. The grown rod was examined under an optical polarization microscope, where differently oriented crystals appear with different colors. Single crystals were identified and extracted based on these images. To prepare powder samples for the x-ray diffraction (XRD) characterization, single crystals were ground into fine powders. The XRD data were collected at room temperature using an x-ray diffractometer (SmartLab SE, Rigaku) with Cu-K_α radiation ($\lambda = 1.54$ Å). The diffraction scan covered the angular range from 10° to 120° with a step size of 0.02° and a scanning rate of 10°/min. The collected XRD data were then subject to Rietveld refinement using the FULLPROF software suite to extract structural parameters, including the occupancy of Cu^{2+} and Ga^{3+} ions at the A and B sites and the inversion parameter δ.

Single crystals were aligned using a Laue x-ray diffractometer and then cut using a wire cutting machine. The dc magnetic susceptibility above 2 K was measured in a commercial Quantum Design physical property measurement system (PPMS), while those below 2 K were measured in a commercial Quantum Design magnetic property measurement system (MPMS) equipped with a He-3 refrigerator module. The ultralow-temperature specific-heat measurements were performed in a PPMS equipped with a dilution refrigerator. AC magnetic susceptibility measurements were performed using both the AC dilution refrigerator (ACDR) and AC measurement system (ACMS) modules of the Quantum Design PPMS. The same sample was measured in both setups to ensure consistency. The ACDR module was used to access the ultralow-temperature regime down to ∼50 mK, while the ACMS measurements were carried out above 1.9 K under identical excitation conditions (2×10^{-4} T). To ensure the accuracy of the low-temperature data, background correction was applied to the ACDR results using the ACMS data as a reference in the overlapping temperature range (from 1.9 to 4.0 K).

Neutron scattering experiments were performed on MACS [39] and SPINS at the NIST Center for Neutron Research, and on SEQUOIA [40] at Oak Ridge National Laboratory. On MACS, the incident energy E_i was fixed to 5 meV. The measurements were conducted by rotating the samples at 0.3, 15, and 100 K, respectively. In the time-of-flight experiment at SEQUOIA, the measurements were made at the base temperature of 5 K with two E_i's of 20 and 40 meV, with a Fermi chopper frequency of 300 Hz, and a scan of rotation about the sample's vertical axis over a range of 154°. Measurements were also performed at $T = 100$ K and used for a quantification of the sample background as described later in the text. The wave vector $\boldsymbol{Q}$ was expressed in reciprocal lattice units (r.l.u.) as (H, K, L), where $a^* = b^* = c^* = 2\pi/a$ with $a = 8.27$ Å in the space group $Fd\bar{3}m$. The sample used for the neutron scattering measurements consisted of 3 rods with a total mass of 19.8 g, and was aligned in the $(HK0)$ scattering plane.

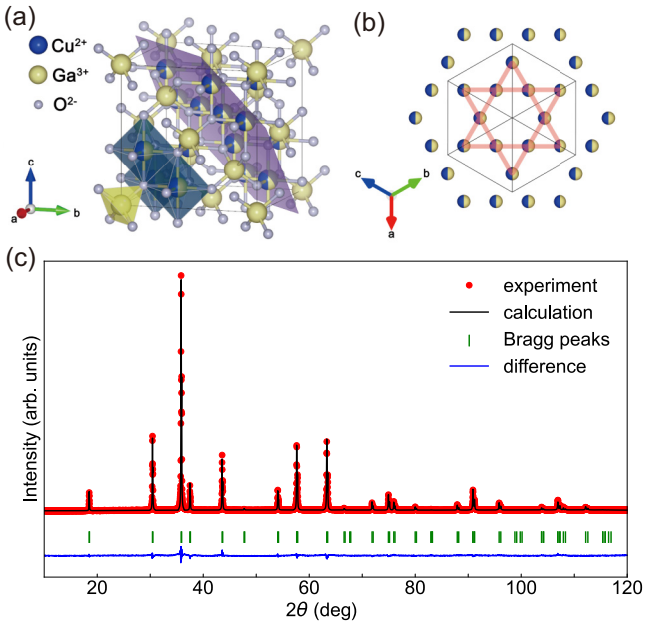


FIG. 1. (a) Schematic illustration of the crystal structure of $CuGa_2O_4$, drawn using VESTA [41]. The tetrahedral environment at the A site and the octahedral environment at the B site are also illustrated. (b) A typical kagome layer viewed along the [111] direction as illustrated by the purple-shaded region in (a). The sphere with mixed blue and yellow colors represents the random occupation of Cu^{2+} and Ga^{3+} ions at these sites. Black lines indicate the boundary of $CuGa_2O_4$'s unit cell. (c) Rietveld refinement results for the powder XRD data collected at room temperature. The red circles and black solid line indicate the measured data and calculated results upon Rietveld refinement, respectively. Green ticks denote Bragg peak positions of $CuGa_2O_4$ with space group $F\bar{3}dm$. The blue solid line represents the difference between the experiment and calculations for this compound.

III. RESULTS

A. Crystal structure and x-ray diffraction

We begin with a detailed description of the structure. Figure 1(a) illustrates the crystal structure of $CuGa_2O_4$, an inverse spinel compound with major Cu^{2+} ions located at the B sites, as indicated by previous powder diffraction studies [42,43]. The A and B sites have tetrahedral and octahedral coordinations, respectively. When viewed along the [111] direction, the ions at the B sites form a kagome plane [highlighted by the purple plane in Fig. 1(a)]. This is a well-known geometrically frustrated network, as shown in Fig. 1(b). Figure 1(c) presents the Rietveld refinement results for the powder XRD data of $CuGa_2O_4$ collected at room temperature. The refinement process was performed under the assumption that there is a small copper vacancy due to vapor loss during the growth procedure, no oxygen vacancy, and a slight crystalline preferred orientation in the powder sample. The fitting results show excellent agreement with the experimental data, as indicated by the minimal residual difference line. The goodness of fit, χ^2, is 3.86, with final refinement parameters $R_p \approx 4.71\%$ and $R_{wp} \approx 6.52\%$. It gives rise to the cubic lattice constant $a = 8.303$ Å. This parameter is in good agreement with those reported in the existing literature [44]. The detailed refinement results are summarized in Table I. The refined site occupancies of Cu^{2+} ions yield a total net occupancy of 0.98 and an inversion parameter $\delta \approx 0.76$, qualitatively consistent with previous studies [42,43].

TABLE I. Refined atomic positions, occupancy (Occ.), and isotropic atomic displacement parameter U_{iso}. The positions of the Cu and Ga ions are fixed based on the symmetry, while those of O are refined.

Atom	Site	x	y	z	Occ.	U_{iso} (Å^2)
Cu (A site)	8*a*	0.00000	0.00000	0.00000	0.24(2)	0.015
Ga (A site)	8*a*	0.00000	0.00000	0.00000	0.76(8)	0.015
Ga (B site)	16*d*	0.62500	0.62500	0.62500	0.61(3)	0.015
Cu (B site)	16*d*	0.62500	0.62500	0.62500	0.37(3)	0.015
O	32*e*	0.37850	0.37850	0.37850	1.000	0.020

The majority of the Cu^{2+} ions occupy the B sites, but fill a minority of these sites, so that the magnetic kagome network is quite disordered. The nearest distance between the B-site ions is 2.935 Å, while the nearest-neighbor and next-nearest-neighbor distances between ions at the A sites are 3.595 Å and 5.871 Å, respectively. The shortest distance between the A and B sites is 3.442 Å. The relatively short distance between nearest-neighbor B sites indicates that the magnetic interactions between B-site Cu^{2+} nearest neighbors likely play a dominant role in determining the magnetic properties of this compound.

B. Magnetic susceptibility and specific heat

To investigate the magnetic properties of $CuGa_2O_4$, the magnetic susceptibility and specific heat have been measured. Figure 2(a) shows the susceptibility curves measured with an external field of 0.1 T applied along the [100] and [111] directions, and perpendicular to the [111] direction. All three curves show no sign of phase transitions as the temperature approaches the lowest value of 2 K. It is noted that there is a slight bifurcation observed at low temperatures among the susceptibility curves measured with different field directions, indicating the presence of weak magnetic anisotropy. We fit the data with the field applied along the [111] direction using the Curie-Weiss law, $1/\chi = (T - \theta_{CW})/C$, over the temperature range from 25 to 100 K, as shown in the inset of Fig. 2(a). This yields a negative Curie-Weiss temperature of $\theta_{CW} \approx -16.11$ K, indicating dominant antiferromagnetic interactions between Cu^{2+} ions. Note that this is an order of magnitude lower than the value of -137 K reported for $CuAl_2O_4$ [26]. The effective moment extracted from the fitted Curie-Weiss constant is approximately 1.71 μ_B/Cu^{2+}, which is comparable to the theoretical value of 1.73 μ_B/Cu^{2+} expected for spin 1/2.

Specific-heat measurements down to ~80 mK at various applied fields along the [100] direction are shown in Fig. 2(b). The data are plotted as C_p/T vs T with a logarithmic scale. We do not attempt to subtract the phonon contribution, as it is expected to be negligible at low temperatures [45,46]. Despite the nuclear Schottky contribution for $T \lesssim 0.2$ K, a broad hump is observed around 1 K at zero field, which shifts to

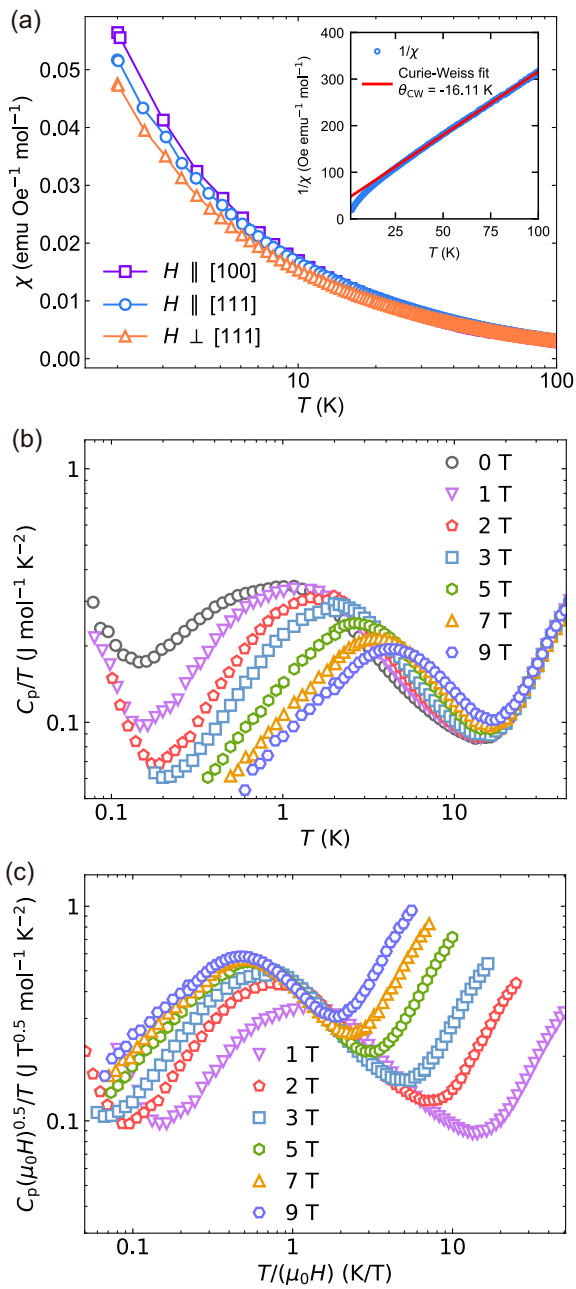


FIG. 2. (a) Susceptibility measured with an external magnetic field of 0.1 T applied parallel to the [100], [111] directions, and perpendicular to the [111] direction. No significant difference is observed in the paramagnetic phase. Inset: The Curie-Weiss fit in the temperature range from 25 to 100 K, which yields a negative Curie-Weiss temperature of −16.11 K, indicating antiferromagnetic interactions in $CuGa_2O_4$. (b) Specific heat measured at different applied magnetic fields. (c) Scaling analysis of the specific heat at different fields ranging from 1 to 9 T.

higher temperatures with increasing applied magnetic fields. Such behavior is typically attributed to the establishment of short-range correlations. This is a common feature in frustrated systems and likewise often found in QSL candidates [45,47,48].

We note that due to the disorder resulting from the interoccupancy between the A and B sites, a random-singlet state may emerge for a frustrated system [49]. To assess this possibility, we perform further analysis upon these data. A random-singlet state is proposed to exhibit a scaling behavior, where the specific-heat data at different applied fields should collapse into a single curve [50,51]. This scaling follows the functional form $\frac{C[H,T]}{T} \sim \frac{1}{H^{\gamma}}[\frac{T}{H}]$ described in Ref. [50]. In Fig. 2(c), we present our data in this form with the parameter $\gamma = 0.5$. Ignoring the phonon-caused upturn for $T/H \gtrsim 1$, we find the data do not collapse into a single curve with a peak as described by the above scaling function, and we have found no improvement by varying γ. This is different from the case of herbertsmithite $ZnCu_3(OH)_6Cl_2$, where the scaling works well [50,52]. These results indicate that the random singlet is not likely to be the ground state for $CuGa_2O_4$.

C. Neutron scattering

To further elucidate the ground state of $CuGa_2O_4$, we conducted both elastic and inelastic neutron scattering (INS) experiments with the spectrometer MACS using single crystals. Figures 3(a) and 3(b) show elastic neutron scattering intensity maps in the $(H, K, 0)$ plane, measured at 0.3 and 100 K, respectively. Compared to 100 K, no additional peaks appear at 0.3 K. To enhance visibility and identify any potential magnetic peaks, we subtract the 100 K data from the 0.3 K data; the results are shown in Fig. 3(c). The resulting difference reveals no authentic signals, but only weak residual intensity, confirming the absence of long-range antiferromagnetic order. These findings suggest that $CuGa_2O_4$ remains magnetically disordered down to at least 0.3 K.

Here, we also probe the low-energy magnetic excitations of $CuGa_2O_4$. Figures 3(d) and 3(e) display INS intensity maps at 2 meV, measured at 0.3 and 100 K, respectively. At 0.3 K, we observe a broad, ringlike continuum of magnetic excitations concentrated around the Brillouin zone boundary, especially for the second Brillouin zone. In contrast, these excitation signals vanish at 100 K, confirming its magnetic origin. To highlight these excitations, we subtract the 100 K data from the 0.3 K data, yielding the net excitation spectra shown in Fig. 3(f). Similar spectra along the Brillouin zone are observed at other energies. The diffuse, continuumlike nature of these excitations is reminiscent of those observed in other QSL candidates, such as herbertsmithite and $YbMgGaO_4$ [9,36,52], where spin fluctuations persist in the absence of a long-range order.

To further confirm the authenticity of these observed magnetic excitation signals, we conducted INS experiments using the time-of-flight spectrometer SEQUOIA. Figures 4(b) and 4(c) show scattering intensity maps in the $(H, K, 0)$ and $(H, K, 1)$ planes at 3 meV, with an energy integrated width of ±0.1 meV. It reveals broad excitation modes similar to those observed in Fig. 3, confirming the nondispersive nature at low energies. By analyzing the dispersion along high-symmetry directions in the Brillouin zone, as indicated in Fig. 4(a), we observe the diffusive low-energy excitations with weak momentum $\boldsymbol{Q}$ dependence [Figs. 4(d) and 4(e)], in stark contrast to well-defined spin waves. The excitation spectra remain continuous over a broad energy range, extending up to approximately 6 meV, with no spin gap observed within the instrumental resolution. To provide further insight into the

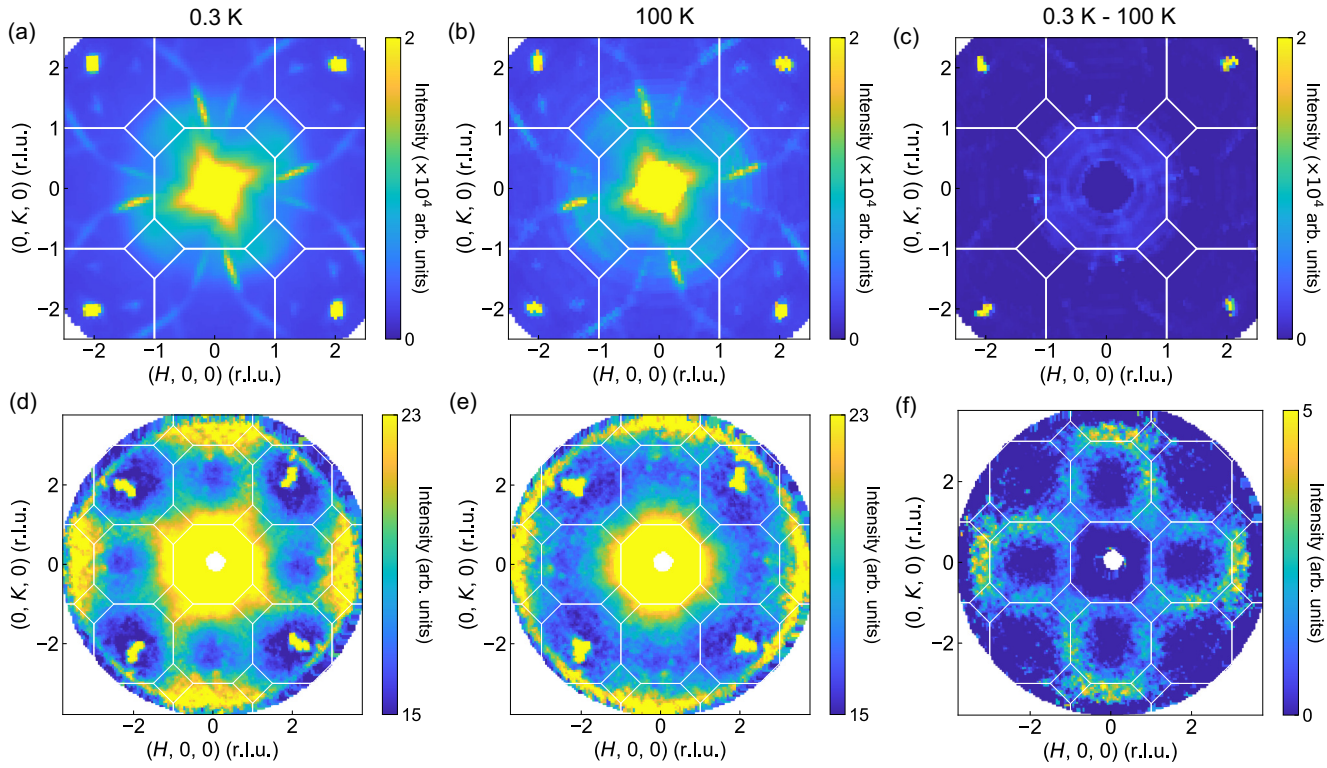


FIG. 3. (a), (b) Elastic neutron scattering data of $CuGa_2O_4$ in the $(H, K, 0)$ plane, measured at 0.3 and 100 K, respectively. (c) Contour map obtained by subtracting the 100 K data from the 0.3 K data. White lines indicate the Brillouin zone boundaries. (d), (e) Inelastic neutron scattering data with an energy transfer of $\Delta E = 2$ meV in the $(H, K, 0)$ plane, measured at 0.3 and 100 K, respectively. (f) Contour map obtained by subtracting the 100 K data from the 0.3 K data. To improve data statistics, all data have been folded according to the fourfold rotational symmetry.

momentum dependence of the excitation spectra, we present constant-energy cuts at 3.6 meV with energy E integrated over 0.6 meV and momentum $\boldsymbol{Q}$ integrated over 0.2 $Å^{-1}$ in perpendicular $\boldsymbol{Q}$ directions, which are shown in Figs. 4(f) and 4(g). The scattering intensity increases as $\boldsymbol{Q}$ moves away from the Γ_2 point towards the high-symmetry points in the first Brillouin zone. The intensity is broadly distributed across the Brillouin zone, with no sharp, well-defined magnon modes.

D. Sub-Kelvin dc and ac susceptibility

The magnetic susceptibility, ultralow-temperature specific heat, and elastic neutron scattering results all point to the absence of long-range magnetic order in $CuGa_2O_4$. In particular, INS reveals a broad, gapless excitation continuum along the Brillouin zone boundary, reminiscent of dynamic spin fluctuations observed in some QSL candidate materials. However, considering the significant antisite disorder between Cu^{2+} and Ga^{3+} ions in this inverse spinel structure (see Table I), the impact of disorder must be carefully evaluated [5,6]. As discussed in Sec. III B, we believe the random-singlet state is less likely according to the scaling analysis of the specific-heat data. Now we turn to assess the possibility of a spin glass, another prevalent case in frustrated systems with strong disorder [54]. In Fig. 5, we plot the dc and ac susceptibility measured below $T = 2$ K. The dc susceptibility data in Fig. 5(a) show that there is a cusp at ∼0.88 K, where the zero-field-cooling (ZFC) and field-cooling (FC) susceptibility curves measured at 0.005 T exhibit a clear bifurcation. This indicates that the system is, in fact, a spin glass, consistent with previous reports on this compound [44,55], albeit with a lower freezing temperature T_f than found in prior measurements. When the applied field is increased to 0.01 T, as shown in the inset of Fig. 5(a), the ZFC and FC curves closely overlap, suggesting the destruction of spin clusters in a spin glass.

To confirm the nature of a spin-glass ground state, we also perform frequency-dependent ac magnetic susceptibility measurements. Figure 5(b) shows the real part of the ac susceptibility $\chi'_{ac}(T)$ with the driving frequency ranging from 464 to 10 000 Hz within 0.5 and 2 K. There is a clear peak around 1 K and it displays a characteristic frequency dependence, consistent with the spin-glass ground state [54,56]. To quantitatively extract the T_f values at various frequencies, we fit the $\chi'_{ac}(T)$ peaks with the temperature range of 0.6 to 1.5 K by using an empirical asymmetric Lorentzian function,

$$\chi'_{ac}(T) = \chi_0 + \frac{A}{1 + \left(\frac{T - T_f}{w[1+\lambda \mathrm{sgn}(T-T_f)]}\right)^2}, \quad (1)$$

where χ_0, A, w, and λ represent the background, peak amplitude, intrinsic half width, and asymmetry of the peak profile, respectively. The sign function $\mathrm{sgn}(T - T_f)$ ensures that the asymmetry is applied correctly across the peak center. It gives rise to a value of $T_f = 0.98$ K for 464 Hz, which is quite close to that of 0.88 K observed in dc magnetic susceptibility measurements. The inset of Fig. 5(b) shows the extracted T_f values

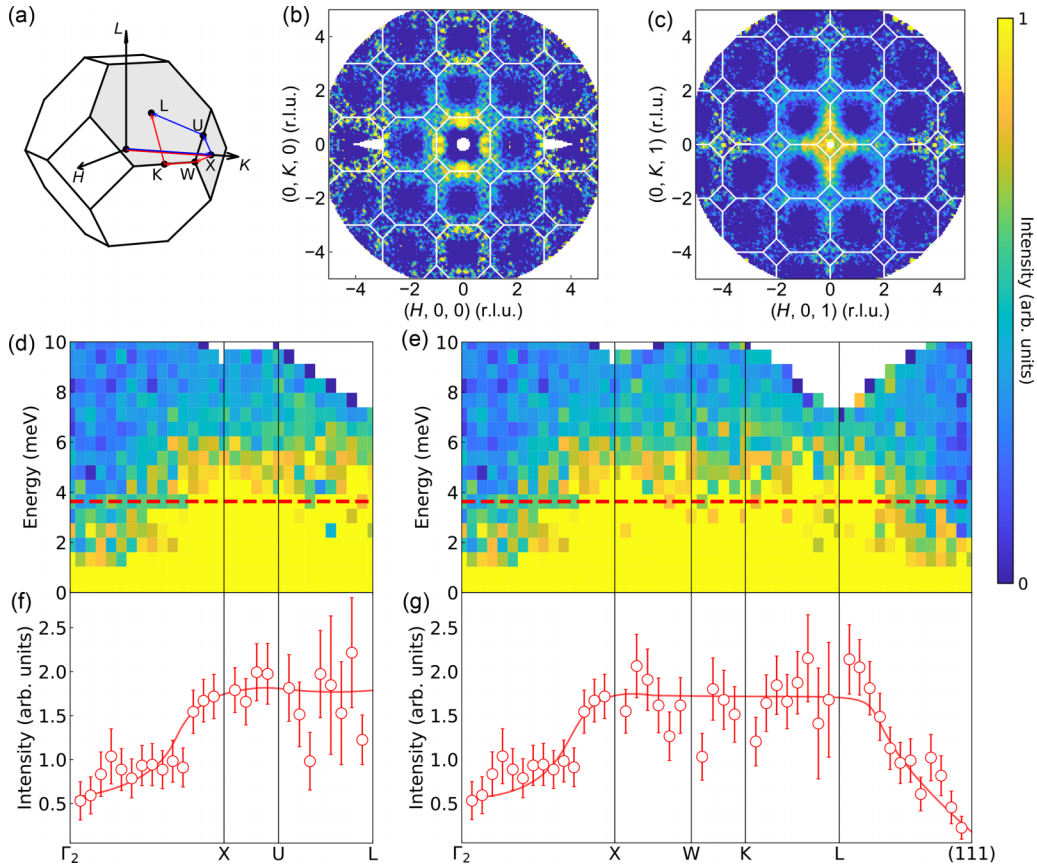


FIG. 4. (a) The first Brillouin zone of $CuGa_2O_4$, with high-symmetry points labeled. (b), (c) Cuts of time-of-flight neutron scattering data in the (H, K, 0) and (H, K, 1) planes, respectively. The energy transfer is 3 meV, with an integrated energy range of ±1 meV and an integrated L range of ±0.25 r.l.u.. To improve the data statistics, the original data have been folded along the [110], [−110], and [010] axes. (d), (e) Low-energy spectra along high-symmetry paths denoted in (a) by the blue and red lines, respectively, generated using the spaghetti_plot method in HORACE [53]. The data are integrated over 0.2 $Å^{-1}$ in perpendicular $\boldsymbol{Q}$ directions. (f),(g) Constant-energy cuts at 3.6 meV with energy integrated over 0.6 meV, as indicated by the red dashed lines in (d) and (e). Error bars indicate one standard deviation ($\pm\sigma$) of the data. The curves over the data points are guides to the eye.

as a function of frequency on a semilogarithmic scale. The relative shift parameter, defined as $\Delta P = \Delta T_f/[T_f \Delta \log(f)]$, is estimated to be 0.061(9), in good agreement with the values reported in other canonical insulating spin-glass systems [56,57].

IV. DISCUSSIONS AND CONCLUSIONS

Via comprehensive measurements using XRD, susceptibility, specific-heat, and neutron scattering techniques, we have shown that although the frustrated inverse-spinel compound $CuGa_2O_4$ exhibits spin-liquid-like behaviors, its ground state is indeed a disorder-induced spin glass. According to the scaling analysis, we do not observe a collapse of the specific-heat data, and therefore we do not consider the ground state to be the random-singlet state [50,58]. We note that in the A-site $CuAl_2O_4$, the tetrahedral symmetry of the dominant magnetic sites is distinct from the present case and could lead to a different ground state [26]. In our case, however, Cu ions mainly occupy the B sites. Under the octahedral crystal-field environment, the e_g orbitals, rather than the t_{2g} orbitals, are active. Such a system is expected to undergo a Jahn-Teller distortion which lifts the degeneracy of the e_g orbitals [59] and prevents the formation of a spin-orbital liquid. Therefore, we do not consider the spin-orbital-liquid ground state here either.

In magnetically frustrated systems, the role of disorder has been extensively studied [47,60,61]. Now, it has been recognized that disorder can often render spin-liquid-like features in a frustrated system [32]. A representative example is the QSL candidate herbertsmithite, where the site mixing between magnetic Cu^{2+} and nonmagnetic Zn^{2+} makes the magnetic excitations mimic those expected for a QSL [62]. $Tm_3Sb_3Zn_2O_{14}$, another material with a kagome structure, which suffers from site-mixing disorder between magnetic Tm^{3+} and nonmagnetic Zn^{2+}, also exhibits properties mimicking characteristics of a QSL state [63,64]. Similarly, a disorder-induced spin excitation continuum has been recently observed in $CoZnMo_2O_7$ [65]. Besides the examples discussed above, in which the antisite disorder arises from the direct transposition between magnetic and nonmagnetic ions, there are also cases without disorder in the magnetic sites, such as $YbMgGaO_4$ and $YbZnGaO_4$ [66–68]. In these materials, disorder stems from the random distribution of nonmagnetic Mg^{2+} (or Zn^{2+}) ions and Ga^{3+}, creating a spatially fluctuating charge environment. Here disorder is believed to

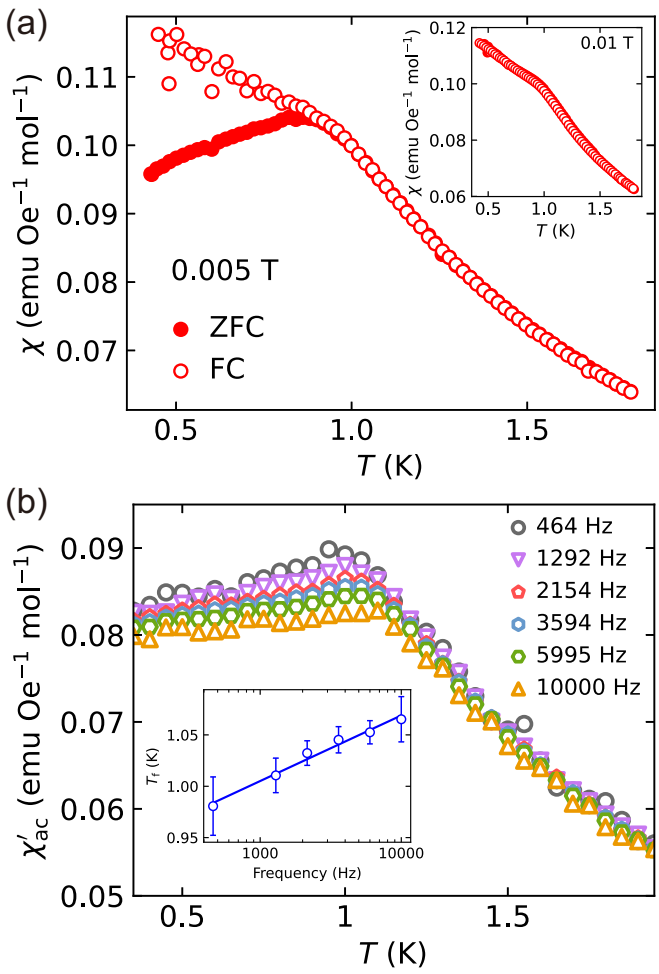


FIG. 5. (a) Temperature dependence of the magnetic susceptibility measured under zero-field-cooling (ZFC) and field-cooling (FC) conditions with a small magnetic field of 0.005 T. A bifurcation at $T_f \approx 0.88$ K is observed. Inset: A similar measurement, but with a 0.01 T field, where no bifurcation between ZFC and FC curves is observed. (b) Real part of the ac magnetic susceptibility χ'_{ac} of $CuGa_2O_4$ measured at various frequencies under an excitation field of 2×10^{-4} T. A clear shift of the freezing temperature T_f toward higher temperatures is observed with increasing frequency, consistent with the spin-glass behavior. Inset: The frequency dependence of T_f plotted on a semilogarithmic scale, where T_f is defined as the temperature corresponding to the peak in $\chi'_{ac}(T)$. The solid line is a guide to the eye.

influence the ground state by randomizing the pseudodipolar interactions of the magnetic ions, thereby promoting QSL-like behaviors [69]. In these samples, the continuous spin excitation spectra observed in the absence of long-range order closely resemble the behaviors seen in $CuGa_2O_4$. These studies highlight that disorder, whether magnetic or nonmagnetic in nature, can induce the spin-liquid-like behaviors in geometrically frustrated materials.

Finally, we would like to compare our results with those reported in Ref. [44], where the spin-glass behavior in $CuGa_2O_4$ was first identified. In that work, the spin-freezing transition was observed at $T_f \approx 2.5$ K based on magnetization, specific-heat, and muon spin relaxation measurements. Our sample shows a lower freezing temperature of $T_f \approx 0.88$ K, which rapidly disappears with the field increasing to 0.01 T. We note that the Curie-Weiss temperature θ_{CW} also exhibits some discrepancy between these two works (−8 K in Ref. [44] vs −16.11 K in this work). This discrepancy may arise from the sensitivity of θ_{CW} to the temperature range used in the Curie-Weiss fitting. For instance, a significantly larger value of $\theta_{CW} \approx -40$ K has been reported when the fitting is performed over a higher-temperature range above 130 K [70]. Moreover, our ac susceptibility measurements show a larger frequency shift parameter [$\Delta P \approx 0.061(9)$] compared to ∼0.026 in Ref. [44]. We attribute these differences to the different degrees of disorder in these samples since the single crystals were prepared by distinct methods. They obtained the samples via the flux method, while we grew single crystals using the floating-zone method with a higher temperature. Considering the comparable ionic radii for Cu^{2+} and Ga^{3+} in both tetrahedral and octahedral coordinations [71], subtle variation in the heat-treated temperature by different means could affect the degree of Cu/Ga site mixing and then the extracted inversion parameters of the samples. Indeed, our structural analysis reveals the inversion parameter $\delta = 0.76$, which is closer to 0.5 than that of 0.84 in Ref. [44], suggesting stronger disorder in our samples. The disorder would disturb the path of magnetic interactions between Cu^{2+} ions and give rise to randomness of exchange interactions. Once the disorder (exchange randomness) reaches a certain level, it would completely destruct the long-range magnetic order and restrict magnetic correlations within short range, giving rise to a spin-glass ground state. Accordingly, the well-defined spin-wave excitations in a magnetically ordered state turn into a continuumlike pattern. Since disorder can drive the system farther away from the magnetically ordered regime, the higher degree of disorder in our samples would lead to lower freezing temperature T_f. Taken together, these data provide solid evidence that $CuGa_2O_4$ hosts a disorder-induced spin-glass ground state. It is also worth noting that theoretical studies suggest that sufficiently dilute impurities can induce order, rather than a disordered state, in spinel compounds [18]. In this context, the degree of disorder is increasingly being recognized as a means to modulate the ground state, rather than being merely an "undesirable" perturbation.

Overall, our comprehensive investigations on the spinel oxide $CuGa_2O_4$, with significant structural disorder, shed light on the intricate interplay between disorder and the ground state. In most cases, structural disorder induces a mimicry of the spin-liquid state rather than a genuine QSL state. In light of this, to find an ideal QSL candidate, it is important to look for materials that are free of structural disorder [6,8,72–74]. For instance, target materials should either have magnetic and nonmagnetic ions occupying separate layers or show a notable mismatch in their ionic radii. Furthermore, materials that have large exchange interactions will also be helpful in realizing the QSL state, as they are more robust to the perturbations and maintain the original QSL state. Along this direction, one can design and explore quantum magnets with shorter and/or more direct exchange paths.

ACKNOWLEDGMENTS

We thank Shun-Li Yu, Jian-Xin Li, and Qingzhen Huang for stimulating discussions. We acknowledge Shichao Li and Shucui Sun from Quantum Design China for the help in measuring the ac susceptibility. This work was supported by the National Key Projects for Research and Development of China with Grants No. 2021YFA1400400 and No. 2024YFA1409200, National Natural Science Foundation of China with Grants No. 12434005, No. 12225407, No. 12204160, and No. 12404173, Postdoctoral Fellowship Program of CPSF under Grant No. BX20240161, China Postdoctoral Science Foundation with Grant No. 2024M751367, Hubei Provincial Natural Science Foundation of China with Grant No. 2025AFB738, Natural Science Foundation of Jiangsu Province with Grants No. BK20241250, No. BK20241251, and No. BK20233001, and Jiangsu Province Excellent Postdoctoral Program with Grant No. 2024ZB021. The work at BNL was supported by the U.S. Department of Energy, Office of Basic Energy Sciences, Contract No. DOE-SC0012704. Neutron scattering experiments were performed on MACS with Proposal No. 26266 and SPINS at the NIST Center for Neutron Research, and SEQUOIA at Oak Ridge National Laboratory with Proposal No. IPTS-24420. Access to MACS was provided by the Center for High Resolution Neutron Scattering, a partnership between the National Institute of Standards and Technology and the National Science Foundation, under Agreement No. DMR-2010792. We acknowledge the support of the National Institute of Standards and Technology, U.S. Department of Commerce, in providing some of the neutron research facilities used in this work. A portion of this research at Oak Ridge National Laboratory's Spallation Neutron Source was sponsored by the U.S. Department of Energy, Office of Basic Energy Sciences. The identification of the x-ray diffractometer (SmartLab SE, Rigaku) and Quantum Design PPMS in this work is solely for the purpose of experimental reproducibility and does not imply endorsement or recommendation by the National Institute of Standards and Technology.

DATA AVAILABILITY

The data that support the findings of this article are not publicly available. The data are available from the authors upon reasonable request.

[1] G. H. Wannier, Antiferromagnetism. The triangular Ising net, Phys. Rev. **79**, 357 (1950).

[2] J. S. Gardner, M. J. P. Gingras, and J. E. Greedan, Magnetic pyrochlore oxides, Rev. Mod. Phys. **82**, 53 (2010).

[3] L. Balents, Spin liquids in frustrated magnets, Nature (London) **464**, 199 (2010).

[4] P. W. Anderson, Resonating valence bonds: A new kind of insulator? Mater. Res. Bull. **8**, 153 (1973).

[5] Y. Zhou, K. Kanoda, and T.-K. Ng, Quantum spin liquid states, Rev. Mod. Phys. **89**, 025003 (2017).

[6] J. Wen, S.-L. Yu, S. Li, W. Yu, and J.-X. Li, Experimental identification of quantum spin liquids, npj Quantum Mater. **4**, 12 (2019).

[7] J. Knolle and R. Moessner, A field guide to spin liquids, Annu. Rev. Condens. Matter Phys. **10**, 451 (2019).

[8] C. Broholm, R. J. Cava, S. A. Kivelson, D. G. Nocera, M. R. Norman, and T. Senthil, Quantum spin liquids, Science **367**, eaay0668 (2020).

[9] T.-H. Han, J. S. Helton, S. Chu, D. G. Nocera, J. A. Rodriguez-Rivera, C. Broholm, and Y. S. Lee, Fractionalized excitations in the spin-liquid state of a kagome-lattice antiferromagnet, Nature (London) **492**, 406 (2012).

[10] J. A. M. Paddison, M. Daum, Z. Dun, G. Ehlers, Y. Liu, M. B. Stone, H. Zhou, and M. Mourigal, Continuous excitations of the triangular-lattice quantum spin liquid $YbMgGaO_4$, Nat. Phys. **13**, 117 (2017).

[11] A. Kitaev, Anyons in an exactly solved model and beyond, Ann. Phys. **321**, 2 (2006).

[12] K. Ran, J. Wang, W. Wang, Z.-Y. Dong, X. Ren, S. Bao, S. Li, Z. Ma, Y. Gan, Y. Zhang, J. T. Park, G. Deng, S. Danilkin, S.-L. Yu, J.-X. Li, and J. Wen, Spin-Wave Excitations Evidencing the Kitaev Interaction in Single Crystalline α-$RuCl_3$, Phys. Rev. Lett. **118**, 107203 (2017).

[13] Y. Shangguan, S. Bao, Z.-Y. Dong, N. Xi, Y.-P. Gao, Z. Ma, W. Wang, Z. Qi, S. Zhang, Z. Huang, J. Liao, X. Zhao, B. Zhang, S. Cheng, H. Xu, D. Yu, R. A. Mole, N. Murai, S. Ohira-Kawamura, L. He, J. Hao, Q.-B. Yan, F. Song, W. Li, S.-L. Yu, J.-X. Li, and J. Wen, A one-third magnetization plateau phase as evidence for the Kitaev interaction in a honeycomb-lattice antiferromagnet, Nat. Phys. **19**, 1883 (2023).

[14] D. Fiorani, J. L. Dormann, J. L. Tholence, and J. L. Soubeyroux, From the antiferromagnetic regime to the spin-glass state in the frustrated spinel system $ZnCr_{2x}Ga_{2-2x}O_4$, J. Phys. C: Solid State Phys. **18**, 3053 (1985).

[15] S.-H. Lee, C. Broholm, W. Ratcliff, G. Gasparovic, Q. Huang, T. H. Kim, and S.-W. Cheong, Emergent excitations in a geometrically frustrated magnet, Nature (London) **418**, 856 (2002).

[16] D. Bergman, J. Alicea, E. Gull, S. Trebst, and L. Balents, Order-by-disorder and spiral spin-liquid in frustrated diamond-lattice antiferromagnets, Nat. Phys. **3**, 487 (2007).

[17] O. Zaharko, A. Cervellino, V. Tsurkan, N. B. Christensen, and A. Loidl, Evolution of magnetic states in frustrated diamond lattice antiferromagnetic $Co(Al_{1-x}Co_x)_2O_4$ spinels, Phys. Rev. B **81**, 064416 (2010).

[18] L. Savary, E. Gull, S. Trebst, J. Alicea, D. Bergman, and L. Balents, Impurity effects in highly frustrated diamond-lattice antiferromagnets, Phys. Rev. B **84**, 064438 (2011).

[19] C. L. Henley, Ordering due to disorder in a frustrated vector antiferromagnet, Phys. Rev. Lett. **62**, 2056 (1989).

[20] N. Tristan, J. Hemberger, A. Krimmel, H A. Krug von Nidda, V. Tsurkan, and A. Loidl, Geometric frustration in the cubic spinels MAl_2O_4(M = Co, Fe, and Mn), Phys. Rev. B **72**, 174404 (2005).

[21] J.-S. Bernier, M. J. Lawler, and Y. B. Kim, Quantum order by disorder in frustrated diamond lattice antiferromagnets, Phys. Rev. Lett. **101**, 047201 (2008).

[22] G. J. MacDougall, D. Gout, J. L. Zarestky, G. Ehlers, A. Podlesnyak, M. A. McGuire, D. Mandrus, and S. E. Nagler, Kinetically inhibited order in a diamond-lattice antiferromagnet, Proc. Natl. Acad. Sci. **108**, 15693 (2011).

[23] O. Zaharko, N. B. Christensen, A. Cervellino, V. Tsurkan, A. Maljuk, U. Stuhr, C. Niedermayer, F. Yokaichiya, D. N. Argyriou, M. Boehm, and A. Loidl, Spin liquid in a single crystal of the frustrated diamond lattice antiferromagnet $CoAl_2O_4$, Phys. Rev. B **84**, 094403 (2011).

[24] M. Iakovleva, E. Vavilova, H.-J. Grafe, S. Zimmermann, A. Alfonsov, H. Luetkens, H.-H. Klauss, A. Maljuk, S. Wurmehl, B. Büchner, and V. Kataev, Ground state and low-energy magnetic dynamics in the frustrated magnet $CoAl_2O_4$ as revealed by local spin probes, Phys. Rev. B **91**, 144419 (2015).

[25] S. Gao, O. Zaharko, V. Tsurkan, Y. Su, J. S. White, G. S. Tucker, B. Roessli, F. Bourdarot, R. Sibille, D. Chernyshov, T. Fennell, A. Loidl, and C. Rüegg, Spiral spin-liquid and the emergence of a vortex-like state in $MnSc_2S_4$, Nat. Phys. **13**, 157 (2017).

[26] R. Nirmala, K.-H. Jang, H. Sim, H. Cho, J. Lee, N.-G. Yang, S. Lee, R. M. Ibberson, K. Kakurai, M. Matsuda, S.-W. Cheong, V. V. Gapontsev, S. V. Streltsov, and J.-G. Park, Spin glass behavior in frustrated quantum spin system $CuAl_2O_4$ with a possible orbital liquid state, J. Phys.: Condens. Matter **29**, 13LT01 (2017).

[27] S. A. Nikolaev, I. V. Solovyev, A. N. Ignatenko, V. Y. Irkhin, and S. V. Streltsov, Realization of the anisotropic compass model on the diamond lattice of Cu^{2+} in $CuAl_2O_4$, Phys. Rev. B **98**, 201106(R) (2018).

[28] H. Y. Huang, A. Singh, C. I. Wu, J. D. Xie, J. Okamoto, A. A. Belik, E. Kurmaev, A. Fujimori, C. T. Chen, S. V. Streltsov, and D. J. Huang, Resonant inelastic x-ray scattering as a probe of $J_{\text{eff}} = 1/2$ state in 3D transition-metal oxide, npj Quantum Mater. **7**, 1 (2022).

[29] H. S. C. O'Neill and A. Navrotsky, Simple spinels; crystallographic parameters, cation radii, lattice energies, and cation distribution, Am. Mineral. **68**, 181 (1983).

[30] R. A. Fregola, F. Bosi, H. Skogby, and U. Hålenius, Cation ordering over short-range and long-range scales in the $MgAl_2O_4$-$CuAl_2O_4$ series, Am. Mineral. **97**, 1821 (2012).

[31] H. Cho, R. Nirmala, J. Jeong, P. J. Baker, H. Takeda, N. Mera, S. J. Blundell, M. Takigawa, D. T. Adroja, and J.-G. Park, Dynamic spin fluctuations in the frustrated A-site spinel $CuAl_2O_4$, Phys. Rev. B **102**, 014439 (2020).

[32] T. Furukawa, K. Miyagawa, T. Itou, M. Ito, H. Taniguchi, M. Saito, S. Iguchi, T. Sasaki, and K. Kanoda, Quantum spin liquid emerging from antiferromagnetic order by introducing disorder, Phys. Rev. Lett. **115**, 077001 (2015).

[33] L. Savary and L. Balents, Disorder-induced quantum spin liquid in spin ice pyrochlores, Phys. Rev. Lett. **118**, 087203 (2017).

[34] K. E. Sickafus, J. M. Wills, and N. W. Grimes, Structure of spinel, J. Am. Ceram. Soc. **82**, 3279 (1999).

[35] P. F. Ndione, Y. Shi, V. Stevanovic, S. Lany, A. Zakutayev, P. A. Parilla, J. D. Perkins, J. J. Berry, D. S. Ginley, and M. F. Toney, Control of the electrical properties in spinel oxides by manipulating the cation disorder, Adv. Funct. Mater. **24**, 610 (2014).

[36] Y. Shen, Y.-D. Li, H. Wo, Y. Li, S. Shen, B. Pan, Q. Wang, H. C. Walker, P. Steffens, M. Boehm, Y. Hao, D. L. Quintero-Castro, L. W. Harriger, M. D. Frontzek, L. Hao, S. Meng, Q. Zhang, G. Chen, and J. Zhao, Evidence for a spinon Fermi surface in a triangular-lattice quantum-spin-liquid candidate, Nature (London) **540**, 559 (2016).

[37] B. Gao, T. Chen, D. W. Tam, C.-L. Huang, K. Sasmal, D. T. Adroja, F. Ye, H. Cao, G. Sala, M. B. Stone, C. Baines, J. A. T. Verezhak, H. Hu, J.-H. Chung, X. Xu, S.-W. Cheong, M. Nallaiyan, S. Spagna, M. B. Maple, A. H. Nevidomskyy, E. Morosan, G. Chen, and P. Dai, Experimental signatures of a three-dimensional quantum spin liquid in effective spin-1/2 $Ce_2Zr_2O_7$ pyrochlore, Nat. Phys. **15**, 1052 (2019).

[38] Z. Zeng, C. Zhou, H. Zhou, L. Han, R. Chi, K. Li, M. Kofu, K. Nakajima, Y. Wei, W. Zhang, D. G. Mazzone, Z. Y. Meng, and S. Li, Spectral evidence for Dirac spinons in a kagome lattice antiferromagnet, Nat. Phys. **20**, 1097 (2024).

[39] J. A. Rodriguez, D. M. Adler, P. C. Brand, C. Broholm, J. C. Cook, C. Brocker, R. Hammond, Z. Huang, P. Hundertmark, J. W. Lynn, N. C. Maliszewskyj, J. Moyer, J. Orndorff, D. Pierce, T. D. Pike, G. Scharfstein, S. A. Smee, and R. Vilaseca, MACS—A new high intensity cold neutron spectrometer at NIST, Meas. Sci. Technol. **19**, 034023 (2008).

[40] G. E. Granroth, A. I. Kolesnikov, T. E. Sherline, J. P. Clancy, K. A. Ross, J. P. C. Ruff, B. D. Gaulin, and S. E. Nagler, SEQUOIA: A newly operating chopper spectrometer at the SNS, J. Phys.: Conf. Ser. **251**, 012058 (2010).

[41] K. Momma and F. Izumi, *VESTA3* for three-dimensional visualization of crystal, volumetric and morphology data, J. Appl. Crystallogr. **44**, 1272 (2011).

[42] J. Lopitaux, J. Arsene, and M. Lenglet, Study of the system $Li_{0.5}Ga_{2.5}O_4$-$CuGa_2O_4$ by IR spectrometry and neutron diffraction, J. Inorg. Nucl. Chem. **38**, 985 (1976).

[43] J. M. R. González and C. O. Areán, X-ray diffraction determination of the cation distribution and oxygen positional parameter in polycrystalline spinels, J. Chem. Soc., Dalton Trans. **1985**, 2155 (1985).

[44] G. A. Petrakovskii, K. S. Aleksandrov, L. N. Bezmaternikh, S. S. Aplesnin, B. Roessli, F. Semadeni, A. Amato, C. Baines, J. Bartolomé, and M. Evangelisti, Spin-glass state in $CuGa_2O_4$, Phys. Rev. B **63**, 184425 (2001).

[45] J. S. Helton, K. Matan, M. P. Shores, E. A. Nytko, B. M. Bartlett, Y. Yoshida, Y. Takano, A. Suslov, Y. Qiu, J.-H. Chung, D. G. Nocera, and Y. S. Lee, Spin Dynamics of the Spin-1/2 Kagome Lattice Antiferromagnet $ZnCu_3(OH)_6Cl_2$, Phys. Rev. Lett. **98**, 107204 (2007).

[46] S. Yamashita, Y. Nakazawa, M. Oguni, Y. Oshima, H. Nojiri, Y. Shimizu, K. Miyagawa, and K. Kanoda, Thermodynamic properties of a spin-1/2 spin-liquid state in a κ-type organic salt, Nat. Phys. **4**, 459 (2008).

[47] Y. Y. Huang, Y. Xu, L. Wang, C. C. Zhao, C. P. Tu, J. M. Ni, L. S. Wang, B. L. Pan, Y. Fu, Z. Hao, C. Liu, J.-W. Mei, and S. Y. Li, Heat transport in herbertsmithite: Can a quantum spin liquid survive disorder? Phys. Rev. Lett. **127**, 267202 (2021).

[48] Z. Ma, S. Zheng, Y. Chen, R. Xu, Z.-Y. Dong, J. Wang, H. Du, J. P. Embs, S. Li, Y. Li, Y. Zhang, M. Liu, R. Zhong, J.-M. Liu, and J. Wen, Possible gapless quantum spin liquid behavior in the triangular-lattice Ising antiferromagnet $PrMgAl_{11}O_{19}$, Phys. Rev. B **109**, 165143 (2024).

[49] I. Kimchi, A. Nahum, and T. Senthil, Valence bonds in random quantum magnets: Theory and application to $YbMgGaO_4$, Phys. Rev. X **8**, 031028 (2018).

[50] I. Kimchi, J. P. Sheckelton, T. M. McQueen, and P. A. Lee, Scaling and data collapse from local moments in frustrated disordered quantum spin systems, Nat. Commun. **9**, 4367 (2018).

[51] C. Peng and L. Zhang, Dynamical scaling behavior of the two-dimensional random singlet state in the random Q model, Phys. Rev. B **110**, 235112 (2024).

[52] T.-H. Han, M. R. Norman, J.-J. Wen, J. A. Rodriguez-Rivera, J. S. Helton, C. Broholm, and Y. S. Lee, Correlated impurities and intrinsic spin-liquid physics in the kagome material herbertsmithite, Phys. Rev. B **94**, 060409(R) (2016).

[53] R.A. Ewings, A. Buts, M.D. Le, J. Van Duijn, I. Bustinduy, and T.G. Perring, Horace: Software for the analysis of data from single crystal spectroscopy experiments at time-of-flight neutron instruments, Nucl. Instrum. Methods Phys. Res., Sect. A **834**, 132 (2016).

[54] K. Binder and A. P. Young, Spin glasses: Experimental facts, theoretical concepts, and open questions, Rev. Mod. Phys. **58**, 801 (1986).

[55] L. A. Fenner, A. S. Wills, S. T. Bramwell, M. Dahlberg, and P. Schiffer, Zero-point entropy of the spinel spin glasses $CuGa_2O_4$ and $CuAl_2O_4$, J. Phys.: Conf. Ser. **145**, 012029 (2009).

[56] J. A. Mydosh, Spin glasses: redux: An updated experimental/materials survey, Rep. Prog. Phys. **78**, 052501 (2015).

[57] K. Mehlawat, G. Sharma, and Y. Singh, Fragile magnetic order in the honeycomb lattice Iridate Na_2IrO_3 revealed by magnetic impurity doping, Phys. Rev. B **92**, 134412 (2015).

[58] D. Bairwa, A. Bandyopadhyay, D. Adroja, G. B. G. Stenning, H. Luetkens, T. J. Hicken, J. A. Krieger, G. Cibin, M. Rotter, S. Rayaprol, P. D. Babu, and S. Elizabeth, Quantum spin liquid ground state in the rare-earth triangular antiferromagnet $SmTa_7O_{19}$, Phys. Rev. B **111**, 104413 (2025).

[59] H. A. Jahn, E. Teller, and F. G. Donnan, Stability of polyatomic molecules in degenerate electronic states - I—Orbital degeneracy, Proc. R. Soc. London, - Math. Phys. Sci. **161**, 220 (1937).

[60] H. Murayama, Y. Sato, T. Taniguchi, R. Kurihara, X. Z. Xing, W. Huang, S. Kasahara, Y. Kasahara, I. Kimchi, M. Yoshida, Y. Iwasa, Y. Mizukami, T. Shibauchi, M. Konczykowski, and Y. Matsuda, Effect of quenched disorder on the quantum spin liquid state of the triangular-lattice antiferromagnet 1*T*-TaS_2, Phys. Rev. Res. **2**, 013099 (2020).

[61] W.-H. Kao and N. B. Perkins, Disorder upon disorder: Localization effects in the Kitaev spin liquid, Ann. Phys. **435**, 168506 (2021).

[62] M. R. Norman, *Colloquium* : Herbertsmithite and the search for the quantum spin liquid, Rev. Mod. Phys. **88**, 041002 (2016).

[63] Z.-F. Ding, Y.-X. Yang, J. Zhang, C. Tan, Z.-H. Zhu, G. Chen, and L. Shu, Possible gapless spin liquid in the rare-earth kagome lattice magnet $Tm_3Sb_3Zn_2O_{14}$, Phys. Rev. B **98**, 174404 (2018).

[64] Z. Ma, Z.-Y. Dong, S. Wu, Y. Zhu, S. Bao, Z. Cai, W. Wang, Y. Shangguan, J. Wang, K. Ran, D. Yu, G. Deng, R. A. Mole, H.-F. Li, S.-L. Yu, J.-X. Li, and J. Wen, Disorder-induced spin-liquid-like behavior in kagome-lattice compounds, Phys. Rev. B **102**, 224415 (2020).

[65] B. Gao, T. Chen, C.-L. Huang, Y. Qiu, G. Xu, J. Liebman, L. Chen, M. B. Stone, E. Feng, H. Cao, X. Wang, X. Xu, S.-W. Cheong, S. M. Winter, and P. Dai, Disorder-induced excitation continuum in a spin-1/2 cobaltate on a triangular lattice, Phys. Rev. B **108**, 024431 (2023).

[66] Y. Shen, Y.-D. Li, H. C. Walker, P. Steffens, M. Boehm, X. Zhang, S. Shen, H. Wo, G. Chen, and J. Zhao, Fractionalized excitations in the partially magnetized spin liquid candidate $YbMgGaO_4$, Nat. Commun. **9**, 4138 (2018).

[67] Z. Ma, J. Wang, Z.-Y. Dong, J. Zhang, S. Li, S.-H. Zheng, Y. Yu, W. Wang, L. Che, K. Ran, S. Bao, Z. Cai, P. Čermák, A. Schneidewind, S. Yano, J. S. Gardner, X. Lu, S.-L. Yu, J.-M. Liu, S. Li, J.-X. Li, and J. Wen, Spin-glass ground state in a triangular-lattice compound $YbZnGaO_4$, Phys. Rev. Lett. **120**, 087201 (2018).

[68] Z. Ma, Z.-Y. Dong, J. Wang, S. Zheng, K. Ran, S. Bao, Z. Cai, Y. Shangguan, W. Wang, M. Boehm, P. Steffens, L.-P. Regnault, X. Wang, Y. Su, S.-L. Yu, J.-M. Liu, J.-X. Li, and J. Wen, Disorder-induced broadening of the spin waves in the triangular-lattice quantum spin liquid candidate $YbZnGaO_4$, Phys. Rev. B **104**, 224433 (2021).

[69] Z. Zhu, P. A. Maksimov, S. R. White, and A. L. Chernyshev, Disorder-induced mimicry of a spin liquid in $YbMgGaO_4$, Phys. Rev. Lett. **119**, 157201 (2017).

[70] T. J. Bullard, M. A. Susner, K. M. Taddei, J. A. Brant, and T. J. Haugan, Magnetic and structural properties of the solid solution $CuAl_{2(1-x)}Ga_{2x}O_4$, Sci. Rep. **11**, 11355 (2021).

[71] R. D. Shannon, Revised effective ionic radii and systematic studies of interatomic distances in halides and chalcogenides, Acta Crystallogr. A **32**, 751 (1976).

[72] W. Liu, Z. Zhang, J. Ji, Y. Liu, J. Li, X. Wang, H. Lei, G. Chen, and Q. Zhang, Rare-earth chalcogenides: A large family of triangular lattice spin liquid candidates, Chin. Phys. Lett. **35**, 117501 (2018).

[73] M. M. Bordelon, E. Kenney, C. Liu, T. Hogan, L. Posthuma, M. Kavand, Y. Lyu, M. Sherwin, N. P. Butch, C. Brown, M. J. Graf, L. Balents, and S. D. Wilson, Field-tunable quantum disordered ground state in the triangular-lattice antiferromagnet $NaYbO_2$, Nat. Phys. **15**, 1058 (2019).

[74] P.-L. Dai, G. Zhang, Y. Xie, C. Duan, Y. Gao, Z. Zhu, E. Feng, Z. Tao, C.-L. Huang, H. Cao, A. Podlesnyak, G. E. Granroth, M. S. Everett, J. C. Neuefeind, D. Voneshen, S. Wang, G. Tan, E. Morosan, X. Wang, H.-Q. Lin, L. Shu, G. Chen, Y. Guo, X. Lu, and P. Dai, Spinon Fermi surface spin liquid in a triangular lattice antiferromagnet $NaYbSe_2$, Phys. Rev. X **11**, 021044 (2021).